Inorganic Chemistry

Article

pubs.acs.org/IC

Eu-MOFs with 2-(4-Carboxyphenyl)imidazo[4,5-*f*]-1,10-phenanthroline and Ditopic Carboxylates as Coligands: Synthesis, Structure, High Thermostability, and Luminescence Properties

Sheng Zhang,[†,‡] Yang Yang,[†,‡] Zheng-Qiang Xia,[†] Xiang-Yu Liu,[†,§] Qi Yang,[†] Qing Wei,[†] Gang Xie,[†] San-Ping Chen,*[,†] and Sheng-Li Gao[†]

[†]Key Laboratory of Synthetic and Natural Functional Molecule Chemistry of Ministry of Education, College of Chemistry and Materials Science, Northwest University, Xi'an, Shaanxi 710069, P. R. China

[§]School of Chemistry and Chemical Engineering, Ningxia University, Yinchuan 750021, China

Supporting Information

ABSTRACT: Hydrothermal reactions of europium(III) salt with 2-(4-carboxyphenyl)imidazo[4,5-*f*]-1,10-phenanthroline and dicarboxylic acid as coligands—benzene-1,4-dicarboxylic acid, 4,4′-biphenyldicarboxylic acid, 2,5-dibromoterephthalic acid, and naphthalene-1,4-dicarboxylic acid—lead to four europium fluorescent materials (**1**−**4**). Structural analyses reveal that **1**−**4** have binuclear 3D metal−organic frameworks with different channels, void volumes, and conjugated structures tuned by ditopic carboxylates. There are no latticed and coordinated water molecules occurring in **1**−**3**, while the free water molecules fill in 1D channels of **4**. **4**′ was readily obtained via water removal of **4**. Thermal analyses of all compounds show the high thermal stability of the main framework up to 450 °C. Optical studies indicate that **1**−**4** and **4**′ show the characteristic red luminescence emission of the Eu^{III} ion in the visible regions at room temperature. On the basis of emission spectra, their luminescence lifetimes were determined. In particular, compound **4**′ shows a longer lifetime (τ = 0.942 ms) and significantly enhanced quantum yield (39%) compared with those of **1** (11%, 0.770 ms), **2** (4%, 0.414 ms), **3** (18%, 0.807 ms), and **4** (26%, 0.858 ms).

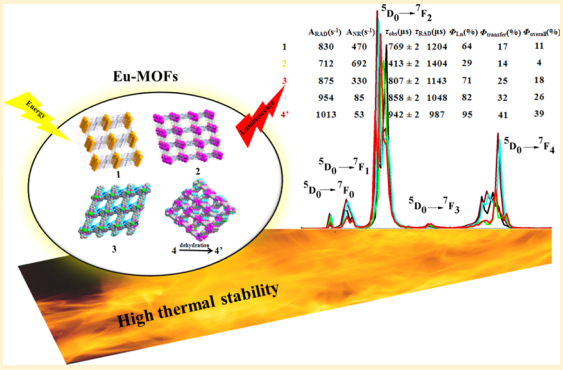

INTRODUCTION

In recent years, lanthanide metal−organic frameworks (Ln-MOFs) have been of intense interest owing to their fantastic topological structures and intriguing photoluminescence.[1−3] The former benefits from the varied coordination geometries and abundant coordination numbers of Ln^{III} ions, while the latter profits from the sharp and long-lifetime characteristic 4f−4f emission bands of Ln^{III} ions because of the shielding of the $5s^25p^6$ filled subshells. Especially, Eu^{III} ions have been regarded as attractive for employment as red emitters in multicolor displays and organic light-emitting diodes.[4] Eu-MOFs may thus become outstanding candidates for exploiting optical devices.[3d] As is known, it is inevitable to face two main problems for the construction of Ln-MOFs.

First, in general, the spin/parity-forbidden nature of the f−f transitions results in abominably low mole extinction coefficients.[5] The characteristic emissions of europium compounds primarily stem from electric-dipole (ED) transitions forbidden by Laporte's rule, associated with the change of parity.[3d,6,7] Nevertheless, when an organic ligand functioning as the sensitizer is introduced to conquer the weak absorption induced by those forbidden rules, transitions become partly permitted because of *J* mixing and the admixture of vibrational states or the states from the surrounding ligand field.[8] So, numerous chromophoric antenna ligands, in particular, π-conjugated organic chromophores,[9] have received the most attention. Herein, long-conjugated multidentate 2-(4-carboxyphenyl)imidazo[4,5-*f*]-1,10-phenanthroline (HNCP) is selected as the main ligand. On the one hand, it has three potential coordination domains to coordinate with the Ln ions, including the bidentate phenanthroline moiety, the amino group of the imidazolyl ring, and the terminal carboxylate group (Scheme 1).[10] When HNCP is used as the bridging ligand, the phenanthroline N and carboxylate O atoms in either end can multiply connect lanthanide metal central ions. On the other hand, it is born with conjunctive aromatic rings, which not only increases the rigidity of the structures but also provides a powerful absorbing sensitizer. Additionally, a certain degree of rigidity and robustness of the phenanthroline moiety are also helpful for keeping the coordination sphere from reducing nonradiative deactivation. These merits lay a solid foundation for the design of compounds with excellent luminescence properties.

Received: May 30, 2014
Published: October 6, 2014

   dx.doi.org/10.1021/ic501253c | *Inorg. Chem.* 2014, 53, 10952−10963

Scheme 1. Diverse Coordination Domains of HNCP[a]

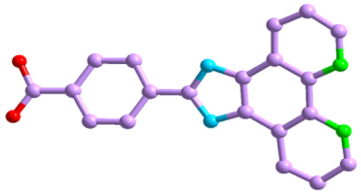

[a]Color code: red, terminal carboxylate group; blue, amino group of the imidazolyl ring; green, bidentate phen moiety.

Scheme 2. Ligands Used in the Paper

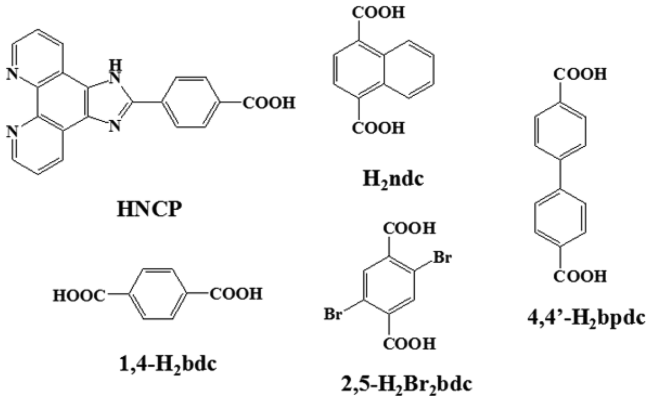

Second, the luminescence properties of Ln-MOFs could be noticeably influenced by the species of guest molecules and the coordination environments of metal centers.[11] According to the theory of hard and soft acids and bases,[12] Ln ions as hard acids are likely to be hard donor atoms, such as O atom. Consequently, the first coordination sphere of Ln^{III} ions is easy to connect with some solvents, especially water molecules. Water molecules are highly effective nonradiative relaxers to quench luminescence because of the loss of excited-state energy from the Ln^{III} ions through the vibration energy of the close-proximity O−H oscillator.[13] Meanwhile, these solvents limit the extension of the dimension of Ln-MOFs and also influence the thermal stability.[11d,13d,14] As is reported many references, MOFs of structure, stability, and function can be tuned via the linker design, such as ditopic carboxylate linkers.[13a,15] The merits are as follows: (1) They can be used as the second ligands to take the solvent's place, force the spatial dimension of the structure to be higher, and further improve the stability of the framework. (2) The 3D Ln-MOF systems can be functionalized with different organic groups of the ligands, such as Br, NH_2, OC_3H_7, OC_5H_{11}, C_2H_4, and C_4H_4. Additionally, their pore sizes could be stretched through long molecular struts, such as biphenyl, tetrahydropyrene, pyrene, and terphenyl. (3) Aromatic carboxylic acids frequently acted as the sensitizers. (4) The carboxyl groups display various coordination modes, affecting intramolecular energy transfer in compounds. Extending the idea above, if ditopic carboxylate linkers are selected as coligands, do the substituents in the aromatic ring and long molecular struts affect the structures and thus the luminescence properties of the final Eu-MOFs?

In this paper, we prepared a series of Eu-MOFs based on the HNCP ligand by introducing various aromatic dicarboxylic acids as coligands (1,4-H_2bdc = benzene-1,4-dicarboxylic acid, 4,4′-H_2bpdc = 4,4′-biphenyldicarboxylic acid, 2,5-H_2Br_2bdc = 2,5-dibromoterephthalic acid, and H_2ndc = naphthalene-1,4-dicarboxylic acid; Scheme 2), aiming to shed some light on new Eu-MOF molecular materials for use in a new generation of miniaturized devices. Fortunately, four new binuclear europium(III) compounds $[Eu(NCP)(L)]_n$ [L = 1,4-H_2bdc (**1**), 2,5-H_2Br_2bdc (**2**), 4,4′-H_2bpdc (**3**)] and $[Eu(NCP)(ndc)(H_2O)_2]_n$ (**4**) based on the HNCP ligand and various second ligands were hydrothermally synthesized and structurally characterized. On the basis of thermal analysis of compound **4**, compound **4′** was readily prepared by guest dehydration of **4**. The luminescence properties of all compounds were discussed.

EXPERIMENTAL SECTION

Materials and Instrumentation. The 2-(4-carboxyphenyl)-imidazo[4,5-*f*]-1,10-phenanthroline (HNCP) ligand was prepared using phenanthren-9-ol as the raw material via a two-step reaction (Scheme 3). The thermogravimetric (TG) data for compounds **1**−**4** and **4′** were collected on a NETZSCH STA 449F3 instrument under a N_2 atmosphere at a heating rate of 10 °C/min from 30 to 1000 °C; an empty Al_2O_3 crucible was used as the reference. Powder X-ray diffraction (PXRD) was carried out on a Bruker D8-ADVANCE diffractometer equipped with Cu Kα at a scan speed of 1°/min. Other chemicals and reagents were obtained by commercial purchase and used without further purification. The ^{1}H NMR spectrum was recorded on an INOVA-400 Varian 400 MHz instrument in a dimethyl sulfoxide (DMSO)-d_6 solution at room temperature. Electrospray ionization mass spectrometry (ESI-MS) spectra were recorded using an HCT mass spectrometer (Bruker Daltonics) under the conditions at which the needle and capillary exit voltages were set to 4 kV and 200 V, respectively; the desolvation chamber temperature was set to 573 K. Elemental analyses (C, H, and N) were performed on an Elementar Vario EL III analyzer. IR spectra were recorded on a Tensor 27 spectrometer (Bruker Optics, Ettlingen, Germany) with pressed KBr pellets in the range of 4000−500 cm^{-1}. Optical diffuse reflectance was carried out with a Shimadzu UV-2450 spectrophotometer. The solid-state photoluminescence analyses and lifetime measurements were performed on an Edinburgh FLSP920 fluorescence spectrometer. The overall quantum yields ($\Phi_{overall}$) were measured by both relative[16] and absolute methods (see the Supporting Information, SI).[17,18]

Synthesis of HNCP. A phenanthren-9-ol oxidation reaction with bis(trifluoroacetoxy)iodobenzene [$(CF_3CO_2)_2IC_6H_5$, BTI] was carried out in aqueous *N*,*N*-dimethylformamide (DMF) at 0 °C, obtaining 10-phenanthroline-5,6-dione. 10-Phenanthroline-5,6-dione (0.1 mmol, 210 mg) was dissolved, together with 4-carboxybenzaldehyde (0.1 mmol, 150 mg), in 10 mL of acetic acid. The mixture system temperature was increased to 100 °C and the mixture stirred for 30 min, to which 1.46 g of dry ammonium acetate (19.0 mmol, 20 equiv) was added with stirring at 120 °C for 2 h. Then the reaction system was reduced to room temperature, filtered, and washed with a lot of water, acetone, and ether to yield the desired product. Yield: 286 mg (88%). Mp: >300 °C. After several days, a few dark-orange HNCP crystals were obtained by slow evaporation of the above filtrate, which was determined by single-crystal X-ray diffraction (Table 1). IR (KBr pellet, cm^{-1}): 3375(b), 3082(b), 2648(b), 2532(b), 1940(w), 1695(s), 1616(m), 1556(s), 1481(m), 1441(m), 1362(m), 1306(s), 1283(m), 1097(s), 959(m), 862(w), 808(s), 716(s), 696(w), 619(m), 525(w), 467(w) (see Figure S1 in the SI). ^{1}H NMR (DMSO-d_6): δ 12.93 (s, 1H), 7.89 (d, 2H), 7.75 (d, 2H), 7.47 (d, 2H), 7.02 (d, 2H), 6.80 (d, 2H) (see Figure S2 in the SI). Anal. Calcd for $C_{20}H_{12}N_4O_2$ (340.34): C, 70.57; H, 3.56; N, 16.47. Found: C, 70.85; H, 3.44; N, 16.91. ESI-MS: *m*/*z* 341.11 (100%; $[M + H]^+$).

Synthesis of [Eu(NCP)(1,4-bdc)]$_n$ (1). $EuCl_3·6H_2O$ (0.0366 g, 0.1 mmol), HNCP (0.0170 g, 0.05 mmol), 1,4-H_2bdc (0.0083 g, 0.05 mmol), acetone (5 mL), and H_2O (1 mL) were mixed and stirred for 20 min. The reaction system above was sealed in a 10 mL Teflon-lined stainless steel autoclave and maintained at 190 °C for 3 days. Upon reduction of the temperature to room temperature at a rate of 5 °C/h, yellow-brown block crystals of compound **1** were gained in 48% yield. Anal. Calcd for $C_{28}H_{15}EuN_4O_6$ (655.40): C, 51.22; H, 2.30; N, 8.54. Found: C, 51.36; H, 2.29; N, 8.60. IR (KBr, cm^{-1}): 3423(b), 2366(w), 1709(m), 1613(s), 1553(s), 1398(b), 1221(w), 1176(w), 1147(w), 1129(w), 1111(w), 1096(w), 1073(m), 1040(w), 1011(w), 977(w),

dx.doi.org/10.1021/ic501253c | *Inorg. Chem.* 2014, 53, 10952−10963

Scheme 3. Synthetic Procedures for the HNCP Ligand

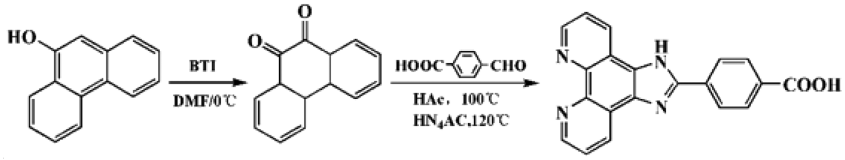

Table 1. Crystal Data and Structure Refinement Summary for the HNCP·3H$_2$O Ligand and Compounds 1−4

	HNCP·3H$_2$O	1	2	3	4
empirical formula	$C_{20}H_{18}N_4O_5$	$C_{28}H_{15}EuN_4O_6$	$C_{28}H_{13}Br_2EuN_4O_6$	$C_{34}H_{19}EuN_4O_6$	$C_{32}H_{21}EuN_4O_8$
fw	394.38	655.40	813.20	731.49	741.49
cryst syst	monoclinic	monoclinic	monoclinic	triclinic	orthorhombic
space group	$P2_1/c$	$c2/c$	$P2_1/n$	$P\bar{1}$	$Pbca$
a (Å)	3.7161(8)	24.1650(15)	10.0700(7)	9.5948(19)	16.6588(15)
b (Å)	24.686(5)	11.2586(7)	23.4076(16)	11.227(2)	17.6541(17)
c (Å)	21.803(4)	20.1253(12)	11.5729(8)	14.752(3)	19.2806(18)
α (deg)	90	90	90	82.390(4)	90
β (deg)	96.552(5)	95.3670(10)	104.6890(10)	83.808(4)	90
γ (deg)	90	90	90	83.401(4)	90
V (Å^3)	1987.0(7)	5451.4(6)	2638.7(3)	1557.7(5)	5670.3(9)
Z	4	8	4	2	8
D_c (g/cm^3)	1.318	1.597	2.047	1.560	1.737
T (K)	296(2)	296(2)	296(2)	296(2)	296(2)
μ (mm^{-1})	0.097	2.349	5.458	2.064	2.274
F(000)	824	2576	1560	724	2944
reflns collected/unique	10699/3903	14428/5367	14099/5122	8303/5984	30226/5848
R(int)	0.1113	0.0362	0.0452	0.0684	0.0985
data/restraints/param	3903/12/263	5367/0/354	5122/0/370	5984/18/382	5848/0/406
GOF on F^2	1.083	1.066	1.017	1.056	1.000
R1[a] [$I > 2\sigma(I)$]	0.0903	0.0390	0.0412	0.1014	0.0435
wR2[b] (all data)	0.3155	0.1577	0.1433	0.2849	0.0928

[a] $R1 = \sum(F_o - F_c)/\sum F_o$. [b] $wR2 = [\sum w(F_o^2 - F_c^2)^2/\sum w(F_o^2)^2]^{1/2}$.

944(w), 882(w), 863(w), 841(m), 807(w), 789(w), 734(m), 694(w), 634(w), 568(w), 524(w).

Synthesis of [Eu(NCP)(2,5-Br$_2$bdc)]$_n$ (2). $EuCl_3·6H_2O$ (0.0366 g, 0.1 mmol), HNCP (0.0170 g, 0.05 mmol), H_2Br_2bdc (0.0156 g, 0.05 mmol), acetone (3 mL), and H_2O (3 mL) were mixed and stirred for 20 min. The system above was sealed in a 10 mL Teflon-lined stainless steel autoclave and maintained at 190 °C for 3 days. After the heat was tardily reduced to room temperature at a rate of 5 °C/h, yellow-brown block crystals of compound **2** were gained in 37% yield. Anal. Calcd for $C_{28}H_{13}Br_2EuN_4O_6$ (813.2): C, 41.39; H, 1.61; N, 6.90. Found: C, 41.36; H, 1.29; N, 6.60. IR (KBr, cm^{-1}): 3415(b), 2360(w), 1681(w), 1601(s), 1575(w), 1555(w), 1535(w), 1479(w), 1452(w), 1392(b), 1326(w), 1280(w), 1243(w), 1194(w), 1137(w), 1097(w), 1071(m), 1044(w), 1018(w), 975(w), 948(w), 882(w), 839(w), 805(w), 759(w), 736(w), 719(m), 643(w), 633(w), 557(w), 530(w).

Synthesis of [Eu(NCP)(4,4′-bpdc)]$_n$ (3). $EuCl_3·6H_2O$ (0.0366 g, 0.1 mmol), HNCP (0.0170 g, 0.05 mmol), 4,4′-H_2bpdc (0.0121 g, 0.05 mmol), DMF (2 mL), and H_2O (4 mL) were mixed and stirred for 20 min. The reaction system was sealed in a 10 mL Teflon-lined stainless steel autoclave and maintained at 170 °C for 3 days. After the heat was tardily reduced to room temperature at a rate of 5 °C/h, orange block crystals of compound **3** were gained in 38% yield. Anal. Calcd for $C_{34}H_{19}EuN_4O_6$ (731.51): C, 55.83; H, 2.62; N, 7.66. Found: C, 55.36; H, 2.92; N, 7.60. IR (KBr, cm^{-1}): 3444(b), 1598(m), 1577(m), 1511(m), 1405(s), 1322(w), 1178(w), 1093(w), 1075(w), 1043(w), 852(w), 814(w), 791(w), 773(w), 718(w), 735(w), 686(w), 641(w), 567(w), 530(w).

Synthesis of [Eu(NCP)(ndc)]$_n$·2nH$_2$O (4). $EuCl_3·6H_2O$ (0.0366 g, 0.1 mmol), HNCP (0.0170 g, 0.05 mmol), H_2ndc (0.0216 g, 0.1 mmol), acetone (1 mL), H_2O (5 mL), and dropping triethylamine (70 μL) were mixed and stirred for 20 min. The system above was sealed in a 10 mL Teflon-lined stainless steel autoclave and maintained at 170 °C for 3 days. After slow cooling to room temperature at a rate of 5 °C/h, yellow block crystals of compound **4** were gained in 38% yield. Anal. Calcd for $C_{32}H_{21}EuN_4O_8$ (741.50): C, 51.83; H, 2.85; N, 7.56. Found: C, 51.63; H, 2.29; N, 7.60. IR (KBr, cm^{-1}): 3421(b), 1617(s), 1550(m), 1468(m), 1428(s), 1370(m), 1274(s), 1214(w), 1189(w), 1156(w), 1104(w), 1079(w), 1041(w), 961(w), 864(w), 835(w), 811(w), 789(w), 771(w), 736(w), 668(w), 640(w), 568(w), 532(w).

Synthesis of 4′. The crystals of compound **4** were put in a drying tubular oven and kept heating at 200 °C for about 0.5 h, and yellow powder of **4′** was gained. Anal. Calcd for $C_{32}H_{17}EuN_4O_6$ (705.50): C, 54.48; H, 2.43; N, 7.94. Found: C, 54.36; H, 2.33; N, 7.78. IR (KBr, cm^{-1}): 1622(s), 1545(m), 1477(m), 1410(s), 1380(m), 1298(s), 1223(w), 1111(w), 1180(w), 1114(w), 1059(w), 1067(w), 955(w), 837(w), 822(w), 866 (w), 777(w), 770(w), 722(w), 651(w), 633(w), 587(w), 520(w).

X-ray Crystallography. Single-crystal X-ray diffraction data for HNCP·3H$_2$O and compounds **1**−**4** were collected on a Bruker SMART APEXII CCD diffractometer, equipped with graphite-monochromatized Mo Kα radiation (λ = 0.71073 Å) using ω and φ scan modes. All of the structures were solved by direct methods and refined with full-matrix least-squares refinements based on F^2 using *SHELXS-97* and *SHELXL-97*.[19] H atoms were placed in geometrically calculated positions. All non-H atoms were refined anisotropically. Detailed crystallographic data and structure refinement parameters of HNCP·3H$_2$O and compounds **1**−**4** are given in Table 1. Selected bond distances, angles, and hydrogen bonds are listed in Tables S1 and S2 in the SI.

RESULTS AND DISCUSSION

Description of the Structures. The ligand HNCP crystallizes in the monoclinic system with space group $P2_1/c$, and the

dx.doi.org/10.1021/ic501253c | Inorg. Chem. 2014, 53, 10952−10963

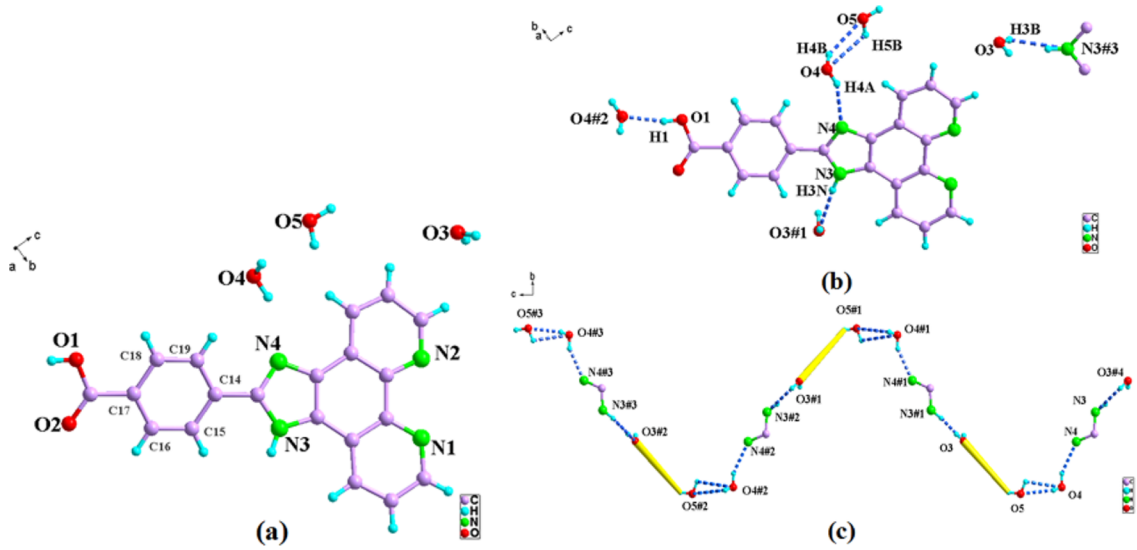

Figure 1. (a) Perspective view of HNCP·3H_2O. (b) Intramolecular hydrogen-bonding interactions in HNCP·3H_2O. (c) Hydrogen-bonding interactions in the 1D chain of HNCP·3H_2O. Yellow sticks point partly to HNCP linkers.

asymmetric unit has three water molecules (Figure 1a). The mean plane of the [4,5-*f*]-1,10-phenanthroline moiety and the benzene ring (C14−C19) form a dihedral angle of 23.48(15)°. As shown in Figure 1b, the O atom (O4) from the free water molecule is located in the plane of the HNCP organic molecule, which links the N atom (N4) from the imidazo group, the O atom (O1) from the carboxylic group, and the O atom (O5) from the other free water molecule by O4−H4A···N4, O1−H1···O4#2, and O4−H4B···O5 bonds to form the intramolecular hydrogen-bond system. The O atom (O3) from another free water molecule and the H atom from the imidazophenantholine ring connect with each other by O3−H3B···N3#3 and N3−H3N···O3#1 hydrogen bonds to generate the other intramolecular hydrogen-bond system. Notably, O3 and N4 are employed as vital atoms of the spacer, which extend the HNCP molecules to shape a boundless 1D zigzag chain via hydrogen-bond systems (Figure 1c). Then, the chains are connected with each other by intermolecular O1−H1···O4#2 hydrogen bonds to yield a 2D network. Furthermore, the hydrogen-bonding and $\pi-\pi$-stacking interactions between the parallel phenanthroline and phenyl rings extend the 2D network to a 3D supermolecular structure. The average distance of $\pi-\pi$ stacking is 3.4473 Å (Figure 2).

Single-crystal X-ray diffraction analysis shows that compounds **1**−**4** have binuclear 3D structures. Compound **1** crystallizes in the monoclinic system with space group *C*2/*c*. As shown in Figure 3a, it contains one Eu^{III} ion, one NCP^- anion, and one 1,4-bdc^{2-} anion in the asymmetric unit. The nine-coordinated Eu^{III} ions are occupied by seven O atoms and two N atoms to generate a distorted three-capped triangular prism (Figure 3b). Two N atoms are from a chelating NCP^- anion [Eu1−N1 = 2.660(4) Å and Eu1−N2 = 2.611(4) Å] and seven O atoms from the carboxylic groups of three μ_2-COO^--bridging 1,4-bdc^{2-} anions [Eu1−O1 = 2.521(3) Å, Eu1−O2 = 2.436(3) Å, Eu1−O5 = 2.348(3) Å, and Eu1−O6 = 2.335(3) Å] and three μ_3-COO^--bridging NCP^- anions [mode I in Scheme 4; Eu1−O4#1 = 2.363(3) Å, Eu1−O4 = 2.612(4) Å, and Eu1−O3 = 2.513(4) Å]. The two neighboring Eu^{III} ions are quadruply bridged by the carboxyl groups from two 1,4-bdc^{2-} and two NCP^- anions to yield a binuclear europium(III) dimer [$Eu_2(COO)_4$; Figure 3c]. In the dimer, the Eu···Eu distance is 3.9265(3) Å. In the whole compound **1**, the N−Eu−N bond angle is 62.29(12)°. The O−Eu−O and O−Eu−N

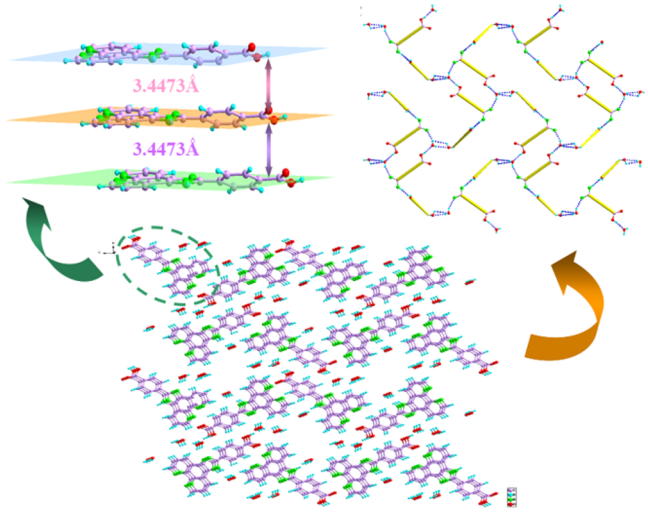

Figure 2. 3D supramolecular network of HNCP·3H_2O.

bond angles are in the ranges of 95.18(14)−103.10(12)° and 71.74(13)−143.16(11)°, respectively. The bond lengths and angles of **1** are in the normal ranges.[20]

These dimers [$Eu_2(COO)_4$] are linked to each other by 2-fold antiparallel NCP^- anions to obtain a 1D double chain (see Figure 3d), in which the face-to-face $\pi-\pi$ interactions between the benzene rings are shown with a distance of 3.5345 Å. Along the *ac* plane, the completely deprotonated 1,4-bdc^{2-} anions connect the 1D chains to form an infinite 2D network structure, and each distorted grid has a size of 20.9997(8) Å × 11.4028(6) Å (Figure 3e). Along the crystallographic *b* axis, the dimers are connected by μ_2-COO^--bridging 1,4-bdc^{2-} anions serving as pillars to enlarge the 2D network structure into a 3D framework, which presents 1D open rhombic channels along every crystallographic orientation of the *a*, *b*, and *c* axes, and no guest molecules encased in them (Figure 3f−h). The rhombic channels own the same size of 11.4028(6) Å × 11.2586(8) Å along crystallographic the *a* and *c* axes, which is slightly smaller than that along the *b* axis. Moreover, the estimated solvent-accessible void volume is 18.3% of the total crystal volume using the *PLATON*/*VOID* routine.[21]

dx.doi.org/10.1021/ic501253c | *Inorg. Chem.* 2014, 53, 10952−10963

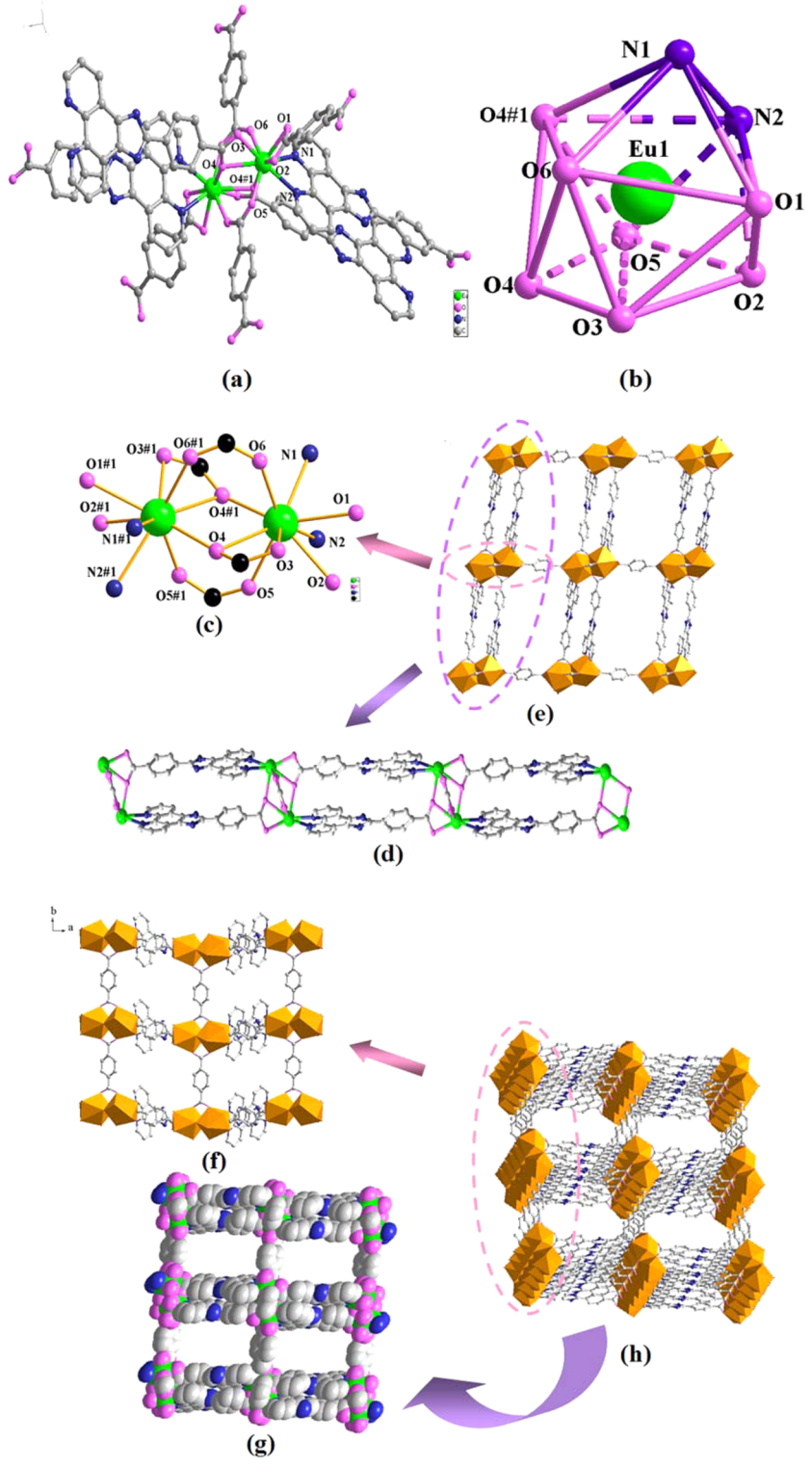

Figure 3. Structure of compound **1**. (a) Coordination environment of the Eu^{III} ion (symmetry code: #1, $-x + 1$, y, $-z + {}^{1}/_{2}$). (b) Coordination polyhedral geometry of the Eu^{III} ion. (c) Dimer of Eu^{III} ions bridged by the carboxyl groups from two 1,4-bdc^{2-} and two NCP^{-} anions. (d) 1D infinite double chain linked by these dimers [$Eu_2(COO)_4$] and 2-fold antiparallel NCP^{-} anions along the b axis. (e) These 1D chains connected by the completely deprotonated 1,4-bdc^{2-} anions to form an infinite 2D network structure in the ac plane. (f) 2D layer in the ab plane. (g) 3D framework assembled via 1,4-H_2bdc ligands along the a axis. (h) Space-filling diagram of the packing down the b axis, showing the rhombic channels [the orange polyhedron stands for the europium(III) dimer]. H atoms are omitted for clarity.

Compound **2** belongs to the monoclinic system with space group $P2_1/n$. As shown in Figure 4a, it contains one Eu^{III} ion, one NCP^{-} anion, and one Br_2bcd^{2-} anion in the asymmetric unit. The central Eu^{III} ion is eight-coordinated through two N and six O atoms from two NCP^{-} and three 2,5-Br_2bcd^{2-} anions to form the coordination sphere (Figure 4a). Two N atoms belong to a chelating NCP^{-} anion [Eu−N1 = 2.529(6) Å and Eu−N2 = 2.587(6) Å], two O atoms belong to the μ_2-COO^{-}-bridging

dx.doi.org/10.1021/ic501253c | *Inorg. Chem.* 2014, 53, 10952−10963

Scheme 4. Two Coordination Modes of HNCP in Compounds 1−4 (M = Metal)

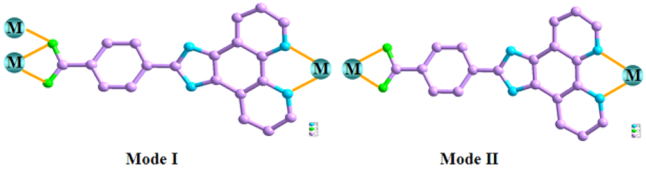

NCP^- anions [Eu−O5 = 2.348(3) Å and Eu−O6 = 2.335(3) Å], and the others belong to three μ_2-COO^--bridging 2,5-Br_2bdc^{2-} anions [Eu−O3 = 2.523(4) Å, Eu−O4 = 2.612(4) Å, Eu−O1 = 521(3) Å, and Eu−O2 = 2.436(3) Å]. Its coordination geometry is a distorted two-capped triangular prism (Figure 4b). In **2**, the N−Eu−N bond angle is 65.01(19)°, which is larger than that of compound **1**. The O−Eu−O and O−Eu−N bond angles are in the ranges of 53.22(17)−146.67(19)° and 69.3(19)−157.48(19)°, respectively. The carboxyl groups of 2,5-H_2Br_2bdc link with two neighboring Eu^{III} ions to produce a dimer, and the distance of Eu···Eu is 5.360(6) Å.

Different from the above compound **1**, the adjacent Eu^{III} ions are linked by the μ_2-COO^--bridging NCP^- anions (mode II) to shape a series of left- and right-handed helical zigzag chains along the *a* axis (Figure 4c). These helical zigzag chains are connected to each other by the μ_2-COO^--bridging 2,5-Br_2bdc^{2-} anions to yield a 1D double chain. The double chains are further connected by the μ_2-COO^--bridging 2,5-Br_2bdc^{2-} anions to generate a 2D-layered structure in the *ab* plane (Figure 4c,d). The 2D structure can be taken as a four-connected 2D (4,4) network using the dimers as nodes (Figure 4d), in which each rhombic grid structure possesses a size of 18.9174(10) Å × 19.7843(71) Å. Along the crystallographic *b* axis, the layers are stacked together through the interlaminar μ_2-COO^--bridging 2,5-Br_2bdc^{2-} anions to obtain a 3D framework.

Compound **3** pertains to the triclinic system with space group $P\bar{1}$. The asymmetric unit contains one Eu^{III} ion, one NCP^- anion, and one 4,4′-$bpdc^{2-}$ anion (Figure 5a). Each Eu^{III} ion is eight-coordinated by the two N atoms from a chelating NCP^- anion (N1 and N2) and the six O atoms from two μ_2-COO^--bridging NCP^- anions (O1 and O2) and two μ_2-COO^--bridging 4,4′-$bpdc^{2-}$ anions (O3, O4, O5, and O6) to shape a distorted two-capped triangular-prismatic EuO_6N_2 polyhedron (Figure 5b). O5 and N1 inhabit the position of the two caps, and N2, O1, O2, O3, O4, and O6 lie in the vertex position of the triangular prism. As shown in Figure 5c, two eight-coordinated Eu^{III} ions are engaged by two carboxylate groups from two NCP^- anions to shape the binuclear dimer [$Eu_2(COO)_2$]. In the dimer, the Eu^{III} ions are coordinated by completely deprotonated 4,4′-$bpdc^{2-}$ and NCP^- anions in a bridging bidentate fashion (mode I in Scheme 4). The average distances of Eu−O and Eu···Eu are 2.294(11) and 5.4271(15) Å, respectively. The axial positions of the paddlewheel are occupied by the N atoms, and the Eu−N bond lengths of the dimer range from 2.504(14) to 2.560(12) Å, which corresponds well to the known Eu^{III}−N bond distances.[20] The N−Eu−N bond angle is 63.4(4)°. The O−Eu−O and O−Eu−N bond angles are in the ranges of 51.9(4)−153.8(5)°and 75.8(4)−156.9(4)°, respectively.

As depicted in Figure 5c, these [$Eu_2(COO)_2$] dimers are linked by two antiparallel NCP^- anions to give rise to a 1D limitless double chain. The double chains are connected by 4,4′-$bpdc^{2-}$ anions to form the 2D honeycomb lamellar rhombic-shaped network (Figure 5d). To better understand the structure of **3** (Figure 5e), the dimer can be regarded as a 4-connected node and the 4,4′-$bpdc^{2-}$ and NCP^- anions act as linkers, which can be considered to simplify the square-grid-like topology with these grids of dimensions of 14.9253(23) Å × 15.5914(24) Å (calculated from the distance of the neighboring Eu^{III} atoms). Furthermore, the 4,4′-$bpdc^{2-}$ anions expand these 2D sheets to a pillar-layered 3D framework (Figure 5f). The 3D topology of **3** is shown in Figure 5g. A broad unoccupied void space [14.9253(23) Å × 15.5914(24) Å × 15.5363(22) Å] exists in **3** (Figure 5h) that is smaller than that of compound **1** (Figure 5g). Because of the torsion of the single bond (C−C) and the various coordination modes of the carboxyl in biphenyldicarboxylic acid, the layers easily tend to intercross in the 3D structure. The theoretical total accessible volume of compound **3** obtained is 16.7% using the *PLATON/VOID* routine.[21]

Compound **4** crystallizes in the orthorhombic system with space group *Pbca*. As shown in Figure 6a, the asymmetric unit contains one Eu^{III} ion, two free water molecules, one NCP^- anion, and one ndc^{2-} anion. The geometrical configuration is defined as a distorted two-capped triangular prism by six O atoms from the carboxyl groups of the NCP^- and ndc^{2-} anions [Eu1−O1 = 2.526(4) Å, Eu1−O2 = 2.411(4) Å, Eu1−O3 = 2.433(4) Å, Eu1−O4 = 2.916(4) Å, Eu1−O5 = 2.365(4) Å, and Eu1−O6 = 2.372(4) Å] and two N atoms from one chelating NCP^- anion [Eu1−N1 = 2.575(4) Å and Eu1−N2 = 2.628(4) Å; Figure 6b]. The two Eu^{III} ions are quadruply bridged by the carboxylate groups of the NCP^- and ndc^{2-} anions to form a binuclear dimer $Eu_2(COO)_4$, and the distance of Eu···Eu is 4.107(4) Å (Figure 6c). It is worth noting that the ndc^{2-} anions not only take part in the bridging of the adjacent Eu^{III} ion but also hold the remaining four sites (Figure 6d). In order to describe the framework of compound **4**, the free water molecules are omitted in the following descriptions. In **4**, the carboxyl groups of HNCP are also completely deprotonated by applying coordination mode II (Scheme 4) and link dimers to shape an infinitely 1D double chain along the crystallographic *a* axis (Figure 6c). These 1D chains are further linked to each other by carboxyl O atoms of ndc^{2-} anions in the *ab* plane to generate a 2D square-grid-like coordination network. The approximate dimensions of these grids are 16.6588(9) Å × 11.6138(9) Å (calculated from the distance of the neighboring Eu^{III} atoms). To simplify the structure of **4**, the two parallel NCP^- and ndc^{2-} anions are considered as one linker, respectively. The $Eu_2(COO)_4$ cluster can be reduced to a 4-connected node, which connects the surrounding $Eu_2(COO)_4$ clusters together by those linkers to generate a 2D network, as shown in Figure 6e. In the vertical direction of the *ab* plane, the remaining four sites in the dimer polyhedron are held by two ndc^{2-} anions (Figure 6f). The ndc^{2-} anions join up with these 2D layers to shape a 3D structure (Figure 6f,g). The space-filling diagram of the packing shows the rhombic channels along the *a* axis (Figure 6h). According to *PLATON* calculations,[21] compound **4** shows a smaller void volume (8.0%) than **1** and **3**.

It is worth noting that these binuclear europium(III) 3D architectures based on the HNCP ligand can be achieved via employment of a different second ligand (dicarboxylic acid). The structural analyses are concluded: (1) HNCP has more potential domains, strong electoral donor atoms (N and O), and V-shaped dicarboxylate, which is beneficial for linking Eu^{III} ions together. (2) The introduction of a second dicarboxylic acid is helpful to extend the structure to higher dimensionality. The sizes, shapes, and substituent groups of the second ligands with various conjugated electronic structures are found to play important

dx.doi.org/10.1021/ic501253c | *Inorg. Chem.* 2014, 53, 10952−10963

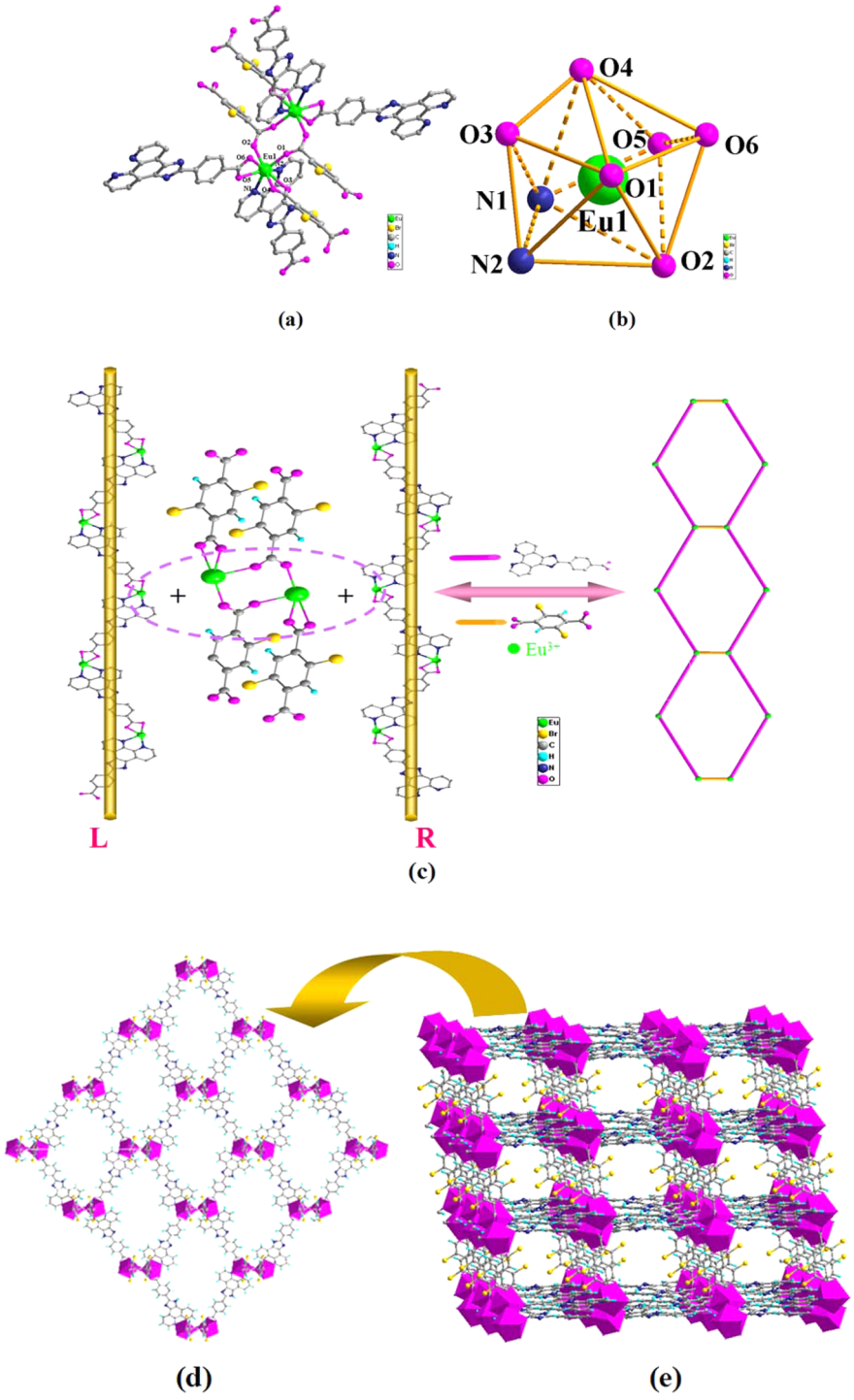

Figure 4. Structure of compound **2**. (a) Coordination environment of the Eu^{III} ion. (b) Coordination polyhedron geometry of the Eu^{III} ion. (c) Adjacent Eu^{III} ions connected by the μ_2-COO^--bridging NCP^- anions (mode II) to shape a series of left- and right-handed helical zigzag chains and further yield a 1D double chain connected by the μ_2-COO^--bridging 2,5-Br_2bdc^{2-} anions along the *a* axis. (d) These double chains connected by the μ_2-COO^--bridging 2,5-Br_2bdc^{2-} anions to generate a 2D-layered structure in the *ab* plane. (e) 2D-layered structure linked by μ_2-COO^- bridging to generate a 3D framework along the *a* axis [the purple polyhedron stands for the europium(III) dimer]. H atoms are omitted for clarity.

roles in tuning the channels, total accessible volumes, and conjugated structures of the compounds, further effecting the luminescence properties of the final Eu-MOFs.

Thermal Analysis and PXRD Results. PXRD experiments were measured for compounds **1**−**4**. The patterns for these compounds are essentially in accordance with the simulated ones from the single-crystal structure analysis, indicating the pure samples of compounds **1**−**4** (Figure S3 in the SI).

To estimate the stabilities of these MOFs, TG analyses of **1**−**4** were carried out in the temperature range of 30−1000 °C at a heating rate of 10 °C/min under a N_2 atmosphere, as shown in Figure 7. The TG curves of **1**−**3** are very similar. **1** is regarded as a representative to analyze the TG performances. The thermal behavior of compound **1** does not show weight loss before 490 °C (470 °C, **2**; 458 °C, **3**; 451 °C, **4**) and exhibits a rather high thermal stability because of no coordinated water molecules

dx.doi.org/10.1021/ic501253c | *Inorg. Chem.* 2014, 53, 10952−10963

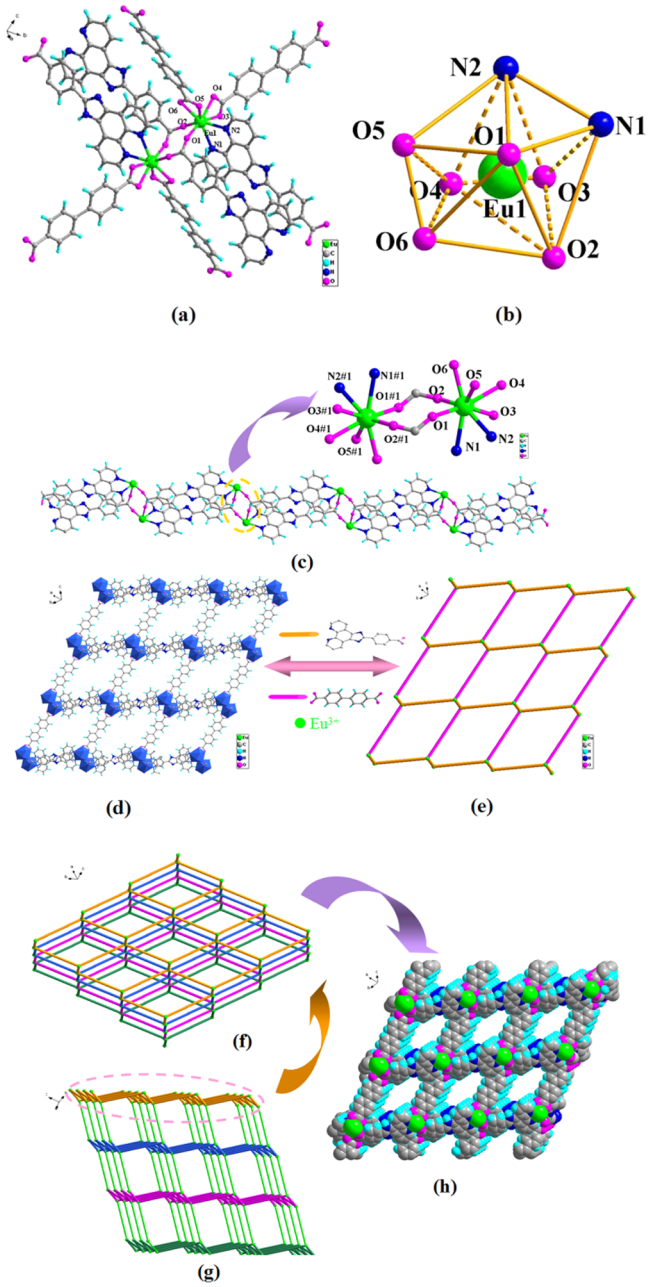

Figure 5. Structure of compound **3**. (a) Coordination environment of the Eu^{III} ion. (b) Coordination polyhedron geometry of the Eu^{III} ion. (c) These $[Eu_2(COO)_2]$ dimers linked by two antiparallel HNCP ligands to give rise to a 1D limitless double chain. (d) Double chains connected by 4,4′-$bpdc^{2-}$ anions to form the 2D honeycomb lamellar rhombic-shaped network [the blue polyhedron stands for the europium(III) dimer]. (e) Schematic illustrating the 2D topology with the dimer as a 4-connected node and the 4,4′-$bpdc^{2-}$ and NCP^{-} anions as linkers. (f) 3D framework assembled via 4,4′-$bpdc^{2-}$ anions. (g) Schematic illustrating the 3D topology (green sticks point to the 4,4′-$bpdc^{2-}$ anion linkers). (h) Space-filling diagram of the packing down the *b* axis, showing the rhombic channels. H atoms are omitted for clarity.

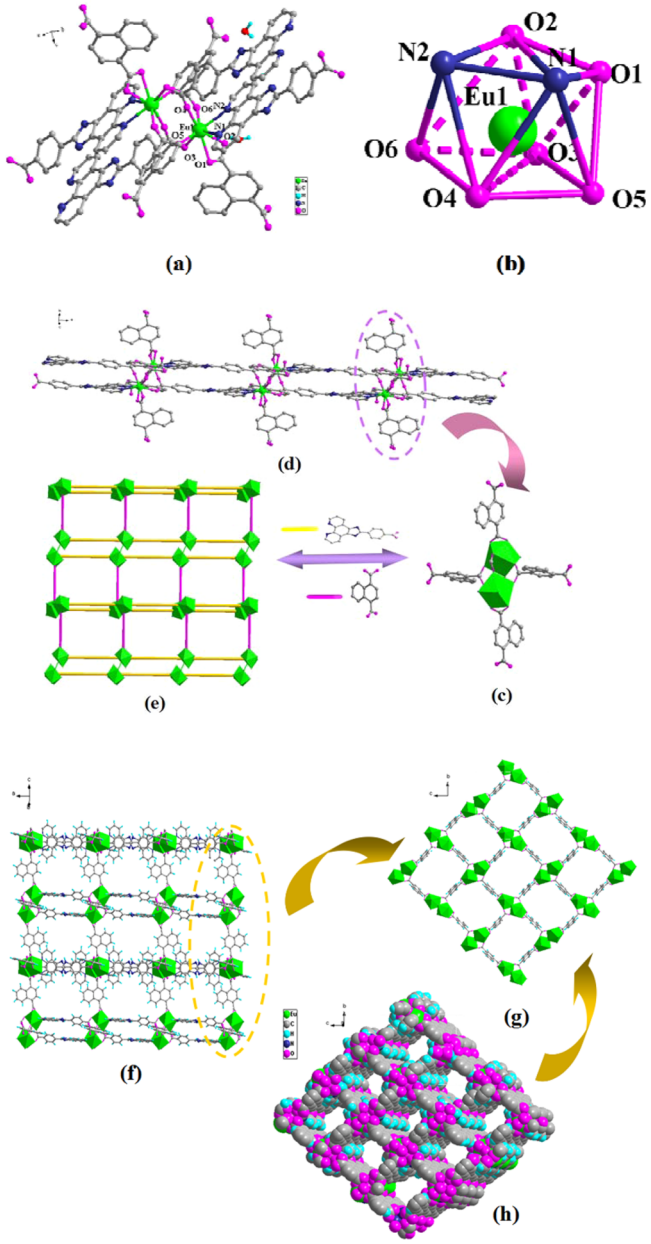

Figure 6. Structure of compound **4**. (a) Coordination environment of the Eu^{III} ion. (b) Coordination polyhedron geometry of the Eu^{III} ion. (c) Eu^{III} ions bridged by the carboxylate groups of NCP^{-} and ndc^{2-} anions to form a binuclear dimer $Eu_2(COO)_4$. HNCP ligands are omitted for clarity. (c) These dimers linked by the carboxyl groups of HNCP to shape an infinitely 1D double chain along the crystallographic *a* axis. (e) Schematic illustrating the 2D topology with two parallel NCP^{-} and ndc^{2-} anions as linkers and the $Eu_2(COO)_4$ cluster as a 4-connected node. (f) 3D framework assembled via ndc^{2-} anions (water molecules are omitted for clarity). (g) Schematic illustrating the 3D topology. (h) Space-filling diagram of the packing down the *a* axis, showing the rhombic channels. H atoms are omitted for clarity.

or solvent molecules in the coordination architectures. Upon an increase in the temperature, the compound experiences a one-step weight loss of 72.51% between 490 and 650 °C, which is ascribed to decomposition of the organic components. The final mass of the residue is 27.49% (21.64%, **2**; 24.92%, **3**) of the original weight, which matches well with the values expected for the formation of Eu_2O_3 (calcd: 26.85%, **1**; 20.65%, **2**; 24.06%, **3**).

Compound **4** displays two steps of weight loss. The first step of weight loss begins at 84 °C and ends at 112 °C. The weight loss of 4.2% corresponds to the removal of two lattice water molecules (calcd 4.8%). Furthermore, the dehydrated compound is stable up to decomposition of the organic components. The decomposition process begins at 450 °C and ends at 585 °C. The final residue (23.92%) could correspond to Eu_2O_3 (calcd 23.73%).

dx.doi.org/10.1021/ic501253c | *Inorg. Chem.* 2014, 53, 10952−10963

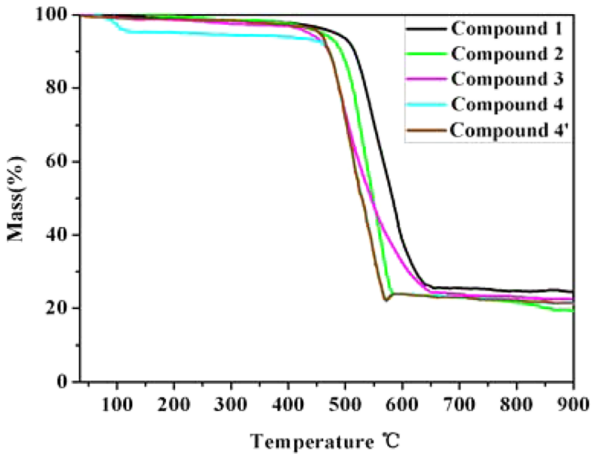

Figure 7. TG analysis curves of compounds **1**−**4** and **4**′.

The DSC curves of compounds **1**−**4** are shown in Figure S4 in the SI. Compounds **1**−**3** show broad upward exothermic peaks, indicating the thermal decomposition processes of one-step weight loss. For compound **4**, the DSC curves present a small downward endothermic peak and a broad upward exothermic peak, which are ascribed to the loss of free water molecules and the decomposition process of the organic components.

In addition, temperature-dependent PXRD (see Figure S5 in the SI) of compounds **1**−**4** after calcination at different elevated temperatures was also studied. The patterns for these compounds closely match the uncalcined compounds before 450 °C. With an increase of the temperature to 500 °C, the characteristic peaks of these compounds are significantly reduced. On the basis of temperature-dependent PXRD and TG analyses of compound **4**, the crystals of **4** are calcined in an oven at 200 °C for about 0.5 h, losing the latticed water molecules and obtaining compound **4**′. IR spectroscopy analysis reveals the absence of the peak at around 3421(b) cm^{-1} in **4**′, indicating no lattice water molecules. The TG curve of **4**′ is very similar to the second step of the TG curve of dehydration of **4** (Figure 7). The PXRD pattern of dehydrated **4** agrees well with that simulated from single-crystal X-ray diffraction data of **4**, which indicates a structural maintenance upon guest water removal (Figure S3 in the SI).

In parallel with TG analysis and temperature-dependent PXRD, IR (see Figure S6 in the SI) and fluorescence (see Figure S7 in the SI) spectra of **1**−**3** and **4**′ after calcination at different elevated temperatures were also studied in order to further prove the thermal stabilities of these europium(III) compounds. In the IR spectrum of these calcined samples, the characteristic bands of the carboxylate groups at ∼1690/∼1400 cm^{-1} for (C═O) stretching or flexural vibrations and amino groups at ∼1300 cm^{-1} for (C−N) stretching vibrations still exist and are identical with those of compounds without calcination. The fluorescence spectrum of these calcined compounds at raised temperature also presents negligible differences. Many phenomena above indicate that the structures of synthetic compounds **1**−**3** and **4**′ are fairly stable up to 450 °C. As a consequence, the Eu^{III}-MOFs of **1**−**3** and **4**′ are excellent candidates for luminescence materials when good thermal stability is demanded.

Photophysical Property. As shown in Figure S8 in the SI, the UV−vis absorption spectra of the free HNCP ligand and compounds **1**−**4** and **4**′ were measured in a DMSO solution (c = 2×10^{-5} M). The absorption maxima for the HNCP ligand is assigned to the singlet−singlet n → π^* or $\pi \rightarrow \pi^*$ electronic transitions.[3d,20] The similar trends in absorption spectra of all compounds and the free ligand indicate that coordination of the Eu^{III} ion does not have an obvious effect on the singlet excited state of the free ligand. However, a slight blue shift is discernible in the absorption maximum of the five compounds (λ_{max} = 293 nm), compared with the absorption maxima of the HNCP ligand (λ_{max} = 307 nm), which could be attributed to the lack of aggregation in the MOFs, whereas the free ligand exhibits a certain degree of π-stacking interactions (Figure 2).[22] The molar absorption coefficients of **1**−**4** and **4**′ at 307 nm of 4.909×10^4, 4.792×10^4, 4.949×10^4, 4.819×10^4, and 4.822×10^4 mol^{-1} cm^{-1}, respectively, are similar to that of the H_2TDC ligand (4.697×10^4 mol^{-1} cm^{-1}), which is consistent with crystallographic analysis. The large molar absorption coefficient of the H_2TDC ligand shows a powerful ability to absorb light.

As shown in Figure 8, the excitation spectra of the HNCP ligand and compounds **1**−**4** and **4**′ were obtained by surveying

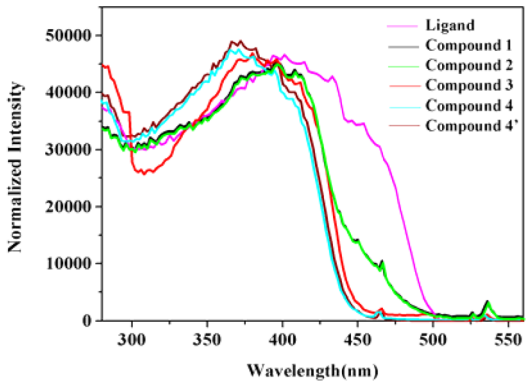

Figure 8. Room temperature excitation spectra for **1**−**4** and **4**′.

the emission wavelength of the Eu^{III} ions at 612 nm in the solid state. They all present a broad excitation band between 300 and 425 nm, which can be assigned to the π−π^* electron transition of the HNCP ligand. Compared with the HNCP ligand, a slight blue shift in the range of 300−425 nm is discernible in their excitation profile, which is ascribed to energy transfer between the HNCP ligand and the Eu^{III} center. The excitation spectra of all compounds display another series of sharp excitation bands with low intensity. These weak signals are characteristic of direct excitation of the Eu^{III} ion, resulting from transitions between the $^7F_0$ and $^5L_6$ states and transitions between the $^7F_{0,1}$ and $^5D_{2,1}$ states.[23] These transitions are overlapped by a broad excitation band, and their intensities are weaker than that of absorption of the organic ligands. It demonstrates that luminescence sensitization by excitation of the ligand is much more efficient than direct excitation of the Eu^{III} ion absorption level.[24]

As shown in Figure 9, the solid-state luminescent properties of compounds **1**−**4** and **4**′ were measured in the range of 500−750 nm at room temperature. The emission spectra of **1**−**4** and **4**′ show the typical europium red emissions under ligand excitation (396 nm). In addition, a series of faint f−f transitions of the Eu^{III} ion at 580, 591, 619, 651, and 699 nm are also observed, corresponding to the $^5D_0 \rightarrow {}^7F_0$, $^5D_0 \rightarrow {}^7F_1$, $^5D_0 \rightarrow {}^7F_2$, $^5D_0 \rightarrow {}^7F_3$, and $^5D_0 \rightarrow {}^7F_4$ transitions, respectively.[25] No broad and strong emission band bridging through the ligand suggests that the absorbed energy is effectively transferred to the emitting level of the Eu^{III} center by the ligand. The weak $^5D_0 \rightarrow {}^7F_0$ and $^5D_0 \rightarrow {}^7F_3$ transitions are regarded as both strictly forbidden in magnetic-dipole (MD) and ED schemes.[26] The $^5D_0 \rightarrow {}^7F_1$ transition is relatively stronger, which is a MD-allowed transition.

dx.doi.org/10.1021/ic501253c | Inorg. Chem. 2014, 53, 10952−10963

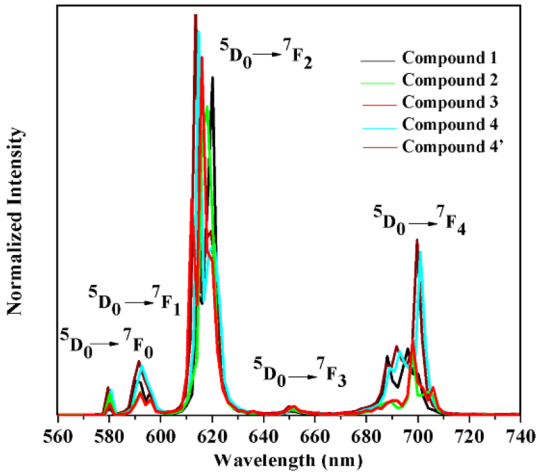

Figure 9. Room temperature emission spectra for **1**–**4** and **4′**.

It is clear that the hypersensitive $^5D_0 \rightarrow {}^7F_2$ transition (ED) displays the highest intensity at 619 nm, indicating the existence of a highly polarizable chemical environment around the Eu^{III} ion. It is documented that the intensity of the $^5D_0 \rightarrow {}^7F_2$ transition increases as the site symmetry of Eu^{III} decreases, while the $^5D_0 \rightarrow {}^7F_1$ transition is MD in origin and insensitive to site symmetry.[27] Obviously, the luminescent intensity ratio of $(^5D_0 \rightarrow {}^7F_2)/(^5D_0 \rightarrow {}^7F_1)$ is 11.50. The results indicate no inversion center in the site of the Eu^{III} ion[28] and a brilliant-red emission of these compounds,[29] matching the single-crystal X-ray analysis of the compounds.

The luminescent decay lifetime measurements of compounds **1**–**4** and **4′** were performed by a pulsed tungsten lamp at room temperature (298 K). Meanwhile, the lifetime values (τ) of the $^5D_0$ level were obtained by fitting with a monoexponential curve. The luminescent decay profiles are shown in Figures S9–S12 in the SI, and the lifetime values are given in Table 2. The

Table 2. Radiative (A_{RAD}) and Nonradiative (A_{NR}) Decay Rates, $^5D_0$ Lifetimes (τ_{obs}), Radiative Lifetimes (τ_{RAD}), Intrinsic Quantum Yields (Φ_{Ln}), Energy-Transfer Efficiencies (Φ_{sen}), and Overall Quantum Yields ($\Phi_{overall}$) for Compounds 1–4 and 4′

compound	A_{RAD} (s^{-1})	A_{NR} (s^{-1})	τ_{obs} (μs)	τ_{RAD} (μs)	Φ_{Ln} (%)	$\Phi_{transfer}$ (%)	$\Phi_{overall}$ (%)
1	830	470	769 ± 2	1204	64	17	11[a]
						19	12[b]
2	712	692	413 ± 2	1404	29	14	4[a]
						14	4[b]
3	875	330	807 ± 2	1143	71	25	18[a]
						27	19[b]
4	954	85	858 ± 2	1048	82	32	26[a]
						34	28[b]
4′	1013	53	942 ± 2	987	95	41	39[a]
						44	42[b]

[a]Relative quantum yield. [b]Absolute quantum yield.

experimental curves fit well with single-exponential decays, which points to a single chemical environment around the Eu^{III} ion. The luminescence lifetimes of compounds **1**–**4** and **4′**, unlike the similarity of their photoluminescence spectra, are quite different (0.770 ms for **1**; 0.414 ms for **2**; 0.807 ms for **3**; 0.858 ms for **4**; 0.942 ms for **4′**). These long lifetimes may be attributed to the strong chelating coordination ability and steric architectonic stabilization of the HNCP ligand, offering an effective pathway of energy transfer. Additionally, no solvent molecules or aqua ligands exist in **1**–**3** and **4′**, which can dramatically reduce the energy loss from high-energy vibrations, such as O–H vibrations.[13]

In order to obtain a better acquaintance of the luminescence efficiencies, the quantum yield is another significant parameter to portray the emission process of the Eu^{III} ion besides the luminescence lifetime, which not only demonstrates the ability of the HNCP ligand sensitizing the emission of the Eu^{III} center but also draws conclusions between the structures and photoluminescence properties.[3d] The overall quantum yield ($\Phi_{overall}$) for an europium(III) compound regards the system as a "black box", in which the inner process is not tangibly measured. Being deemed as the compound absorbing a photon (i.e., the antenna is excited), $\Phi_{overall}$ can be calculated as[30]

$$\Phi_{overall} = \Phi_{overall}\Phi_{Ln} \quad (1)$$

where $\Phi_{transfer}$ and Φ_{Ln} correspond to the efficiency of energy shifting from the ligand to the Eu^{III} ion and the intrinsic quantum yield of the Ln ion, respectively. Φ_{Ln} can be defined as

$$\Phi_{Ln} = \frac{A_{RAD}}{A_{RAD} + A_{NR}} = \frac{\tau_{obs}}{\tau_{RAD}} \quad (2)$$

In eq 2, A_{RAD}, A_{NR}, τ_{obs}, and τ_{RAD} represent the radiative decay rate, nonradiative decay rate, $^5D_0$ lifetimes, and radiative lifetimes, respectively.

The intrinsic quantum yields of the Eu^{III} ion could not be decided experimentally upon direct f–f excitation in view of the very low absorption intensity. Consequently, the radiative lifetimes of Eu ($^5D_0$) are calculated from eq 3,[31]

$$A_{RAD} = \frac{1}{\tau_{RAD}} = A_{MD,0}n^3\left(\frac{I_{TOT}}{I_{MD}}\right) \quad (3)$$

Here, $A_{MD,0}$ is the deactivation rate related to the spontaneous emission probability for the $^5D_0 \rightarrow {}^7F_1$ transition in vacuum, equal to 14.65 s^{-1}; n is the refractive index of the medium, which equals 1.5 in the solid sample used in the calculation for coordination compounds; I_{tot}/I_{MD} signifies the ratio of the total area of the integrated $^5D_0 \rightarrow {}^7F_J$ ($J = 0$–4) emissions of the corrected europium(III) emission spectrum to the area of the intensity of the MD $^5D_0 \rightarrow {}^7F_1$ transition.[32] For compounds **1**–**4** and **4′**, the calculated values of A_{RAD}, A_{NR}, and τ_{RAD} via eq 3 are given in Table 2, combined with the lifetime values (τ) of the $^5D_0$ level, and finally the Φ_{Ln} calculated values are 64%, 29%, 71%, 82%, and 95%, respectively.

Compound **1** exhibits slightly higher luminescence efficiency compared with **2**. On the basis of their structures, the poor luminescence efficiency noted in compound **2** may be attributed to the electron-accepting group (Br) of ditopic carboxylate linkers involving in the coordination sphere of **2**, which easily causes fluorescence quenching to reduce the fluorescence quantum yield of the Eu^{III} ion. Moreover, the richer π-conjugated 1,4-H_2bdc second ligand than 2,5-H_2Br_2bdc influences $\Phi_{transfer}$. **3**, **4**, and **4′** exhibit relatively high quantum yields and radiative decay rates because of the distorted eight-coordinated dodecahedral environment of the Eu^{III} ion.[33] In this coordinate environment, the hypersensitive $^5D_0 \rightarrow {}^7F_2$ ED transition is allowed by symmetry-related selection rules and occurs quite easily. So, the inner coordination sphere may result in a following increase in the overall quantum yield. The nonradiative decay rates of **3**, **4**, and **4′** decrease by 29%, 82%, and 89% approximately, compared to that of **1**, because of the extended conjugate system through

dx.doi.org/10.1021/ic501253c | Inorg. Chem. 2014, 53, 10952–10963

the introduction of one phenyl group in the 4 or 2 positions and 4 and 2 positions of the 1,4-H_2bdc ligand. However, it is obvious that the quantum yields of **4** and **4′** are superior to that of **3**, which is probably due to H_2ndc containing a better delocalized conjugated system in contrast to 4,4′-H_2bpdc, leading to a significant enhancement in the overall quantum yield and sensitization and thus resulting in a more efficient ligand-to-metal and less nonradiative $^5D_0$ relaxation process. Noticeably, the photoluminescent properties of **4′** (the dehydrated product of **4**) are obviously modified, along with enhancement of the intensity of the emission bands and an increase in the lifetime and quantum yield to 0.942 ms and 39%. This phenomenon is attributed to the quenching effect of the luminescent state through high-frequency-vibrating water molecules.[13] Compound **4** has a higher quantum yield and longer lifetime than those for the other compounds besides **4′**, despite the presence of solvent molecules in compound **4**. The better delocalized conjugated system possibly compensates for the quenching effect of the uncoordinated water molecules in the channels.

In a word, the quantum yields and lifetimes of compounds **1**−**4** and **4′** follow a sequence of **4′** > **4** > **3** > **1** > **2**, which emphasizes the significant impact of the different sizes, shapes, and substituent groups of ditopic carboxylate linkers and the latticed water molecules on luminescent properties. Additionally, the energy gap between the ligand triplet state and the lowest-lying excited state of the Eu^{III} ion, the coordinated solvent molecules, and the conjugation effect of chromophores and/or coligands also generate cooperative effects in the luminescence properties of Eu-MOFs, as evidenced by reported Eu-MOFs (see Table S3 in the SI).

CONCLUSION

A series of 3D binuclear Eu^{III}-MOFs have been successfully designed and synthesized based on the HNCP ligand with different aromatic dicarboxylic acids as coligands under hydrothermal conditions, which show different channels, void volumes, and conjugated structures tuned by these coligands. The rigidity of the HNCP ligand and the introduction of bicarboxylic acid ligands favor the formation of coordination polymers with high thermal stability. Thermal analyses state that compounds **1**−**4** and the dehydrated product **4′** of **4** have remarkable thermal stabilities of the main framework until 450 °C. The fluorescence spectra of eurpopium(III) compounds **1**−**4** and **4′** exhibit the characteristic red luminescence emission of the Eu^{III} ion in the visible regions at room temperature. The strong chelating coordination ability and steric architectonic stabilization of the HNCP ligand may offer an effective path of energy transfer. A detailed photophysical study shows that the $^5D_0$ quantum efficiency and lifetime of the compounds vary considerably, relying on the introduction of these second ligands: 1,4-H_2bdc ($\Phi_{overall}$ = 11%, τ_{obs} = 0.770 ms, **1**), 2,5-H_2Br_2bdc ($\Phi_{overall}$ = 4%, τ_{obs} = 0.414 ms, **2**), 4,4′-H_2bpdc ($\Phi_{overall}$ = 18%, τ_{obs} = 0.807 ms, **3**), and H_2ndc ($\Phi_{overall}$ = 26%, τ_{obs} = 0.858 ms, **4**; $\Phi_{overall}$ = 39%, τ_{obs} = 0.942 ms, **4′**). Obviously, the lifetime and quantum yield of **4′** increase by 0.084 s and 13%, respectively, compared to those of **4**. The enhancement of the intensity of emission bands and an increase of the lifetime and quantum yield are due to the quenching effect of the luminescent state by high-frequency-vibrating water molecules.

In summary, in the molecular self-organization system of Eu^{III}-ion-based MOFs, the HNCP ligand, ditopic carboxylate linkers, and latticed water molecules have an important influence on the final structures and photoluminescence properties. Meanwhile, it presents an ingenious design to adjust MOF-based fluorescent materials.

ASSOCIATED CONTENT

Supporting Information

X-ray crystallographic files (CIF), selected bond lengths and angles, hydrogen-bonding intereactions, photoluminescence properties, IR, ^{1}H NMR, solid-state emission, and UV−vis absorption spectra, PXRD patterns, DCS plots, and luminescence decay profiles. This material is available free of charge via the Internet at http://pubs.acs.org. Crystallographic data for the structures reported in this paper are also deposited in the Cambridge Crystallographic Data Center with CCDC reference numbers 949867, 948244, 948245, 948246, and 948430 for the HNCP ligand and compounds **1**−**4**, respectively.

AUTHOR INFORMATION

Corresponding Author

*E-mail: sanpingchen@126.com or sanpingchen312@gmail.com. Tel.: +86(29)81535025. Fax: +86(29)81535025.

Author Contributions

‡These authors have equal contribution to this work.

Notes

The authors declare no competing financial interest.

ACKNOWLEDGMENTS

We gratefully acknowledge financial support from the National Natural Science Foundation of China (Grants 21127004, 21203149, 21373162, 21173168, and 21463020) and the Nature Science Foundation of Shanxi Province (Grants FF10091, SJ08B09, and 11JS110).

REFERENCES

(1) (a) Shi, F. N.; Cunha-Silva, L.; Ferreira, R. A. S.; Mafra, L.; Trindade, T.; Carlos, L. D.; Paz, F. A. A.; Rocha, J. *J. Am. Chem. Soc.* **2008**, *130*, 150−167. (b) Eliseeva, S. V.; Bünzli, J. C. G. *Chem. Soc. Rev.* **2010**, *39*, 189−227. (c) Parker, D. *Coord. Chem. Rev.* **2000**, *205*, 109−130. (d) Bochkarev, M. N. *Chem. Rev.* **2002**, *102*, 2089−2118.

(2) (a) Auzel, F. *Chem. Rev.* **2004**, *104*, 139−174. (b) Bünzli, J. C. G.; Pigue, C. *Chem. Soc. Rev.* **2005**, *34*, 1048−1077.

(3) (a) Wong, W. K.; Yang, X. P.; Jones, R. A.; Rivers, J. H.; Lynch, V.; Lo, W. K.; Xiao, D.; Oye, M. M.; Holmes, A. L. *Inorg. Chem.* **2006**, *45*, 4340−4345. (b) Guo, X. M.; Guo, H. D.; Fu, L. S.; Carlos, L. D.; Ferreira, R. A. S.; Sun, L. N.; Deng, R. P.; Zhang, H. J. J. *Phys. Chem.* **2009**, *113*, 12538−12545. (c) Long, J.; Chelebaeva, E.; Larionova, J.; Guari, Y.; Ferreira, R. A. S.; Carlos, L. D.; Paz, F. A. A.; Trifonov, A.; Guérin, C. *Inorg. Chem.* **2011**, *50*, 9924−9926. (d) Gai, Y. L.; Jiang, F. L.; Chen, L.; Bu, Y.; Su, K. Z.; Al-Thabaiti, S. A.; Hong, M. C. *Inorg. Chem.* **2013**, *52*, 7658−7665. (e) Chen, Z.; Zhao, B.; Zhang, Y.; Shi, W.; Cheng, P. *Cryst. Growth Des.* **2008**, *8*, 2291−2298.

(4) (a) Huignard, A.; Gacoin, T.; Boilot, J. P. *Chem. Mater.* **2000**, *12*, 1090−1094. (b) Maggini, L.; Mohanraj, J.; Traboulsi, H.; Parisini, A.; Accorsi, G.; Armaroli, N.; Bonifazi, D. *Chem.—Eur. J.* **2011**, *17*, 8533−8537. (c) Shelton, A. H.; Sazanovich, I. V.; Weinstein, J. A.; Ward, M. D. *Chem. Commun.* **2012**, *48*, 2749−2751. (d) Cui, Y. J.; Xu, H.; Yue, Y. Y.; Guo, Z. Y.; Yu, J. C.; Chen, Z. X.; Gao, J. K.; Yang, Y.; Qian, G. D.; Chen, B. L. *J. Am. Chem. Soc.* **2012**, *134*, 3979−3982.

(5) (a) Carnall, W. T.; Gruen, D. M.; McBeth, R. L. *J. Phys. Chem.* **1962**, *66*, 2159−2164. (b) Kim, Y. H.; Baek, N. S.; Kim, H. K. *ChemPhysChem* **2006**, *7*, 213−221.

(6) (a) Chen, X. Y.; Liu, G. K. *J. Solid State Chem.* **2005**, *178*, 419−428. (b) Van Vleck, J. H. *J. Phys. Chem.* **1937**, *41*, 67−80.

(7) (a) Ofelt, G. S. *J. Chem. Phys.* **1962**, *37*, 511−520. (b) Judd, B. R. *Phys. Rev.* **1962**, *127*, 750−761.

(8) (a) De Bettencourt-Dias, A.; Viswanathan, S. *Dalton Trans.* **2006**, *34*, 4093−4103. (b) Viswanathan, S.; De Bettencourt-Dias, A. *Inorg. Chem.* **2006**, *45*, 10138−10146. (c) Weissman, S. I. *J. Chem. Phys.* **1942**, *10*, 214−217. (d) De Lill, D. T.; De Bettencourt-Dias, A.; Cahill, C. L. *Inorg. Chem.* **2007**, *46*, 3960−3965. (e) Crosby, G. A.; Alire, R. M.; Whan, R. E. *J. Chem. Phys.* **1961**, *34*, 743−748. (f) Leonard, J. P.; Gunnlaugsson, T. J. *Fluorescence* **2005**, *15*, 585−595. (g) Moore, E. G.; Samuel, A. P. S.; Raymond, K. N. *Acc. Chem. Res.* **2009**, *42*, 542−552.

(9) (a) Dong, Y. B.; Wang, P.; Ma, J. P.; Zhao, X. X.; Wang, H. Y.; Tang, B.; Huang, R. Q. *J. Am. Chem. Soc.* **2007**, *129*, 4872−4873. (b) Liu, T. F.; Zhang, W. J.; Sun, W. H.; Cao, R. *Inorg. Chem.* **2011**, *50*, 5242−5248. (c) Chandler, B. D.; Cramb, D. T.; Shimizu, G. K. H. *J. Am. Chem. Soc.* **2006**, *128*, 10403−10412. (d) Borkowski, L. A.; Cahill, L. *Cryst. Growth Des.* **2006**, *6*, 2248−2259. (e) Jia, L. N.; Hou, L.; Wei, L.; Jing, X. J.; Liu, B.; Wang, Y. Y.; Shi, Q. Z. *Cryst. Growth Des.* **2013**, *13*, 1570−1576.

(10) (a) De Mello Donegá, C.; Alves, S., Jr.; De Sá, G. F. *Chem. Commun.* **1996**, 1199−1200. (b) Carlos, L. D.; De Mello Donegá, C.; Albuquerque, R. Q.; Alves, S., Jr.; Menezes, J. F. S.; Malta, O. L. *Mol. Phys.* **2003**, *101*, 1037−1045. (c) Ambili Raj, D. B.; Biju, S.; Reddy, M. L. P. *Dalton Trans.* **2009**, 7519−7528.

(11) (a) Stein, G.; Wurzburg, E. J. *Chem. Phys.* **1975**, *62*, 208−213. (b) Dew, W. H., Jr.; Sudnick, D. R. *J. Am. Chem. Soc.* **1979**, *101*, 334−340. (c) Liu, T. F.; Zhang, W. J.; Sun, W. H.; Cao, R. *Inorg. Chem.* **2011**, *50*, 5242−5248. (d) Richardson, F. S. *Chem. Rev.* **1982**, *82*, 541−552. (e) Zhang, H. B.; Li, N.; Tian, C. B.; Liu, T. F.; Du, F. L.; Lin, P.; Li, Z. H.; Du, S. W. *Cryst. Growth Des.* **2012**, *12*, 670−678.

(12) (a) Nag, A.; Kovalenko, M. V.; Lee, J. S.; Liu, W. Y.; Spokoyny, B.; Talapin, D. V. *J. Am. Chem. Soc.* **2011**, *133*, 10612−10620. (b) Villanneau, R.; Ben Djamaa, A.; Chamoreau, L. M.; Gontard, G.; Proust, A. *Eur. J. Inorg. Chem.* **2013**, 1815−1820. (d) Zhang, J.; Zheng, B.; Zhao, T. T.; Li, G. H.; Huo, Q. S.; Liu, Y. L. *Cryst. Growth Des.* **2014**, *14*, 2394−2400.

(13) (a) Cui, Y. J.; Yue, Y. F.; Qian, G. D.; Chen, B. L. *Chem. Rev.* **2012**, *112*, 1126−1162. (b) Biju, S.; Ambili Raj, D. B.; Reddy, M. L. P.; Kariuki, B. M. *Inorg. Chem.* **2006**, *45*, 10651−10660. (c) Ghorai, S. K.; Samanta, S. K.; Mukherjee, M.; Sardar, P. S.; Ghosh, S. *Inorg. Chem.* **2013**, *52*, 1476−1487. (d) Ambili Raj, D. B.; Silvanose, B.; Reddy, M. L. P. *Dalton Trans.* **2009**, 7519−7528. (e) Sun, H. L.; Yin, D. D.; Chen, Q.; Wang, Z. Q. *Inorg. Chem.* **2013**, *52*, 3582−3584. (f) Xia, J.; Zhao, B.; Wang, H. S.; Shi, W.; Ma, Y.; Song, H. B.; Cheng, P.; Liao, D. Z.; Yan, S. P. *Inorg. Chem.* **2007**, *46*, 3450−3458. (g) Zhao, Y.; Jiao, C. Q.; Sun, Z. G.; Zhu, Y. Y.; Chen, K.; Wang, C. L.; Li, C.; Zheng, M. J.; Tian, H.; Sun, S. H.; Chu, W. *Cryst. Growth Des.* **2012**, *12*, 3191−3199.

(14) (a) Ma, S. Q.; Wang, X. S.; Yuan, D. Q.; Zhou, H. C. *Angew. Chem., Int. Ed.* **2008**, *47*, 4130−4133. (b) Lill, D. T.; Cahill, C. L. *Chem. Commun.* **2006**, 4946−4948.

(15) (a) Lu, W. G.; Wei, Z. W.; Gu, Z. Y.; Liu, T. F.; Park, J. H.; Park, J.; Tian, J.; Zhang, M. W.; Zhang, Q.; Gentle, T., III; Boscha, M.; Zhou, H. C. *Chem. Soc. Rev.* **2014**, *43*, 5561−5593. (b) Tan, Y. X.; He, Y. P.; Zhang, J. *Inorg. Chem.* **2012**, *51*, 9649−9654.

(16) Bril, A.; De Jager-Veenis, A. W. *J. Electrochem. Soc.* **1976**, *123*, 396−398.

(17) De Mello, C.; Wittmann, H. F.; Friend, R. H. *Adv. Mater.* **1997**, *9*, 230−232.

(18) Saleesh Kumar, N. S.; Varghese, S.; Rath, N. P.; Das, S. *J. Phys. Chem. C* **2008**, *112*, 8429−8437.

(19) (a) Sheldrick, G. M. *SHELXS-97, Program for Solution of Crystal Structures*; University of Göttingen: Göttingen, Germany, 1997. (b) Sheldrick, G. M. *SHELXL-97, Program for Refinement of Crystal Structures*; University of Göttingen: Göttingen, Germany, 1997.

(20) Xia, Z. Q.; Wei, Q.; Yang, Q.; Qiao, C. F.; Chen, S. P.; Xie, G.; Zhang, G. C.; Zhou, C. S.; Gao, S. L. *CrystEngComm* **2013**, *15*, 86−99.

(21) (a) Biju, S.; Ambili Raj, D. B.; Reddy, M. L. P.; Kariuki, B. M. *Inorg. Chem.* **2006**, *45*, 10651−10660. (b) Li, X.; Sun, H. L.; Wu, X. S.; Qiu, X.; Du, M. *Inorg. Chem.* **2010**, *49*, 1865−1871. (c) Wan, Y. H.; Zheng, X. J.; Wang, F. Q.; Zhou, X. Y.; Wang, K. Z.; Jin, L. P. *CrystEngComm* **2009**, *11*, 278−283.

(22) Wei, Z.; Gu, Z. Y.; Arvapally, R.; Chen, Y. P.; McDougald, R.; Yakovenko, A.; Feng, D.; Omary, M.; Zhou, H. C. *J. Am. Chem. Soc.* **2014**, *136*, 8269−8276.

(23) Spek, A. L. *PLATON*; The University of Utrecht: Utrecht, The Netherlands, 1999.

(24) Pavithran, R.; Saleesh Kumar, N. S.; Biju, S.; Reddy, M. L. P.; Junior, S. A.; Freire, R. O. *Inorg. Chem.* **2006**, *45*, 2184−2192.

(25) Xia, J.; Zhao, B.; Wang, H. S.; Shi, W.; Ma, Y.; Song, H. B.; Cheng, P.; Liao, D. Z.; Yan, S. P. *Inorg. Chem.* **2007**, *46*, 3450−3458.

(26) (a) Ambili Raj, D. B.; Biju, S.; Reddy, M. L. P. *Inorg. Chem.* **2008**, *47*, 8091−8100. (b) Werts, M. H. V.; Jukes, R. T. F.; Verhoeven, J. W. *Phys. Chem. Chem. Phys.* **2002**, *4*, 1542−1548.

(27) Zhao, Y.; Jiao, C. Q.; Sun, Z. G.; Zhu, Y. Y.; Chen, K.; Wang, C. L.; Li, C.; Zheng, M. J.; Tian, H.; Sun, S. H.; Chu, W. *Cryst. Growth Des.* **2012**, *12*, 3191−3199.

(28) (a) Bünzli, J. C. G.; Piguet, C. *Chem. Soc. Rev.* **2005**, *34*, 1048−1077. (b) Sun, Y. Q.; Zhang, J.; Chen, Y. M.; Yang, G. Y. *Angew. Chem., Int. Ed.* **2005**, *44*, 5814−5817.

(29) (a) Li, Y.; Zheng, F. K.; Liu, X.; Zou, W. Q.; Guo, G. C.; Lu, C. Z.; Huang, J. S. *Inorg. Chem.* **2006**, *45*, 6308−6316. (b) Cheng, J. W.; Zheng, S. T.; Ma, E.; Yang, G. Y. *Inorg. Chem.* **2007**, *46*, 10534−10538.

(30) (a) Xiao, M.; Selvin, P. R. *J. Am. Chem. Soc.* **2001**, *123*, 7067−7073. (b) Comby, S.; Imbert, D.; Chauvin, A. S.; Bünzli, J. C. G.; Charvonnière, L. J.; Ziessel, R. F. *Inorg. Chem.* **2004**, *43*, 7369−7379. (c) Quici, S.; Cavazzini, M.; Marzanni, G.; Accorsi, G.; Armaroli, N.; Ventura, B.; Barigelletti, F. *Inorg. Chem.* **2005**, *44*, 529−537.

(31) (a) Viswanathan, S.; De Bettenacourt-Dias, A. *Inorg. Chem.* **2006**, *45*, 10138−10146. (b) Kim, Y. H.; Baek, N. S.; Kim, H. K. *ChemPhysChem* **2006**, *7*, 213−221.

(32) (a) Chauvin, A. S.; Gumy, F.; Imbert, D.; Bunzli, J. C. G. *Spectrosc. Lett.* **2007**, *40*, 193−193. (b) Chauvin, A. S.; Gumy, F.; Imbert, D.; Bünzli, J. C. G. *Spectrosc. Lett.* **2004**, *37*, 517−532.

(33) Pinsky, M.; Avnir, D. *Inorg. Chem.* **1998**, *37*, 5575−5582.